Natural Hazards **27:** 231–255, 2002.

Fire Danger Monitoring Using ERS-1 SAR Images in the Case of Northern Boreal Forests

BRIGITTE LEBLON*
Remote Sensing and GIS Research Group, Faculty of Forestry and Environment Management, University of New Brunswick, Fredericton, New Brunswick, E3B 6C2, Canada (E-mail: bleblon@unb.ca)

ERIC KASISCHKE
Department of Geography, University of Maryland, College Park, MD, USA

MARTY ALEXANDER
Canadian Forest Service, Edmonton, Alberta, Canada

MARK DOYLE and MELISSA ABBOTT
Remote Sensing and GIS Research Group, Faculty of Forestry and Environment Management, University of New Brunswick, Fredericton, New Brunswick, Canada

(Received: 21 July 2000; accepted: 8 November 2001)

Abstract. Research was carried out to assess the potential of imaging radar systems for monitoring forest fire danger. In Canada, daily forest fire danger ratings are generated by the Canadian Forest Fire Danger Rating System (CFFDRS), based on estimates of fire weather indices (FWI) and measured foliar moisture content (FMC). To evaluate the potential of imaging radar, an experiment was conducted using test sites consisting of jack pine, black spruce and white spruce stands located in the MacKenzie river basin, Northwest Territories, Canada. Radar image intensity values from ERS-1 SAR imagery collected over these stands in 1994 were compared to FWI indices and FMC data. FWI indices were calculated using data from local weather stations. Seasonal trends in radar backscatter (σ^0) were shown to correlate with temperature and precipitation. Significant relationships were found between σ^0 and FWI codes and indices, particularly in the case of the black spruce stands, with slow-drying fuels, like duff moisture code (DMC), drought code (DC), and build-up index (BUI). Rates of changes in σ^0 were related to rates of changes in FMC, particularly in the case of the jack pine stands for old FMC and in the case of white spruce stands for composite FMC.

Key words: fire danger, fire weather index, foliar moisture content, black spruce, jack pine, white spruce, ERS-1 SAR images, Northwest Territories.

1. Introduction

Ignition and spread of forest fires depends on four main factors: (i) the state and nature of the fuel, i.e., proportion of live or dead vegetation, compactness, morphology, species, density, stratification and moisture content; (ii) the physical environment, i.e., weather conditions and topography; (iii) ignition sources (hu-

* Author for correspondence.

man or lightning) and (iv) levels of fire prevention and suppression. The spatial and long-term variability of fire danger is related to fuel types and topography, whereas the temporal and short-term variability is related to fuel moisture content and weather conditions. In Canada, daily fire danger ratings are generated using a semi-empirical modular system known as the Canadian Forest Fire Danger Rating System (CFFDRS) (Stocks *et al.*, 1989). It combines, through simulated indices, weather, fuel, topography and ignition parameters. The simulation is based on moisture physics and heat transfer theory as well as empirical relationships derived from data gathered from experimental fires and well-documented prescribed fires and wildfires.

One of the CFFDRS subsystems, the Fire Weather Index (FWI) system, provides numerical ratings of relative mid-afternoon fire potentials, based solely on air temperature, wind, relative humidity and rainfall data recorded daily at noon local standard time (e.g., Canadian Forest Service, 1987). It considers one single fuel type, i.e., a generalized pine forest (similar to the jack and lodgepole pine types), and three fuel layers described by codes: (a) the fine-fuel moisture code (FFMC) for the fine surface litter, foliage, and small branches; (b) the duff moisture code (DMC) for the loosely-compacted duff of moderate depth; and (c) the drought code (DC) for the deep organic matter of the soil (Canadian Forest Service, 1987; Stocks *et al.*, 1989). The three fuel layers differ as a function of the drying rate measured by the time-lag period, i.e., the time it takes to lose two-thirds of the free moisture at equilibrium, when the air temperature is 20 °C and the relative humidity is 40%. FFMC is related to fast-drying fuels with a time lag of half days, whereas DMC and DC are related to slow-drying fuels, with time-lag periods of twelve days for DMC and of twenty-five days for DC (Canadian Forest Service, 1987). The three codes are then combined into three indices: the build-up index (BUI), the initial spread index (ISI) and the fire weather index (FWI).

Another CFFDRS subsystem, the Fire Behavior Prediction (FBP) system, predicts fire behavior for different fuel types, as a function of: (i) weather records, (ii) topography, (iii) ignition variables and (iv) foliar moisture content (FMC in % dry weight) because of its relationship with crown fire (e.g., Canadian Forest Service, 1992).

Both CFFDRS subsystems have the limitation of not being able to consider variations in environmental conditions at finer spatial scales, but only produce estimates for large geographic regions. This is because the FWI subsystem does not account for the difference in forest types and is dependent on weather records from widely dispersed stations. In the FBP system, fuel types represent broad categories and the approach used to estimate FMC is a generalized semi-empirical method that does not account for the spatial variability among different forest types nor the temporal variability associated with climate and plant phenology.

Information derived from satellite systems offers the potential to address both of these limitations. This rapidly-developing technology offers the advantages of consistent, repeatable, large-area coverage, and can easily provide information

from remote regions. In addition, remote sensing data represent in essence the integrated response of the vegetation to the different factors influencing its status as a fuel base for wildland fires. CFFDRS parameters that can be potentially monitored using satellite data include fuel type and fuel moisture, and plant phenology. In previous studies reviewed in Leblon (2001), fuel moisture has been estimated both from NOAA-AVHRR normalized difference vegetation index (NDVI) images and NOAA-AVHRR thermal infrared imagery, because of the relationship between surface temperatures and plant dryness.

The one primary disadvantage of the AVHRR-derived information is that coverage is restricted to cloud-free conditions, a limitation that can be overcome using data acquired by active microwave sensors (e.g., the imaging radar systems onboard the ERS and Radarsat satellites). In addition, imaging radar systems are very sensitive to variations in the moisture conditions of the vegetation canopy, as well as the ground layer in open canopied forests. Studies have shown that imaging radars are sensitive to soil moisture variations in burned boreal forests (Kasischke *et al.*, 1995a; French *et al.*, 1996; Wang *et al.*, 2000) and in pine stands with low biomass levels (Wang *et al.*, 1994). Saatchi and Moghaddam (2000) demonstrated a relationship between canopy moisture and radar image intensity in jack pine forests. Finally, because of these sensitivities, Bourgeau-Chavez *et al.*, (1999) demonstrated that variations in radar image intensity were positively correlated with fuel moisture indices derived for black spruce forests in interior Alaska.

The goal of our study was to further evaluate the potential of using imaging radar systems to assess canopy and forest fuel moisture conditions of northern boreal forests. With data acquired during the 1994 fire season over Northwest Territories (Canada) in black spruce, jack pine and white spruce stands, our study first investigated how the observed seasonal variations of radar image intensity (measured as radar backscatter or σ^0 are related to the climate parameters used to compute the fuel moisture codes. Second, the relationship between seasonal variations in σ^0 and the FWI codes and indices (FFMC, DMC, DC, BUI and FWI) as well as in FNC was explored, considering the influences of tree type, biomass and surface roughness as represented in the different forest stands.

2. Background on Imaging Radars

Studies have shown that radar backscatter (σ^0) measurements of forested areas depend on (i) vegetation type, species, and structure (e.g., Leckie, 1990; Dobson *et al.*, 1992, 1995a, b), (ii) vegetation biomass (Kasischke *et al.*, 1995b; Harrell *et al.*, 1995, 1997; Pulliainen *et al.*, 1996; Saatchi and Moghaddam, 2000), (iii) topography and surface roughness (e.g., Franklin *et al.*, 1995; Wang *et al.*, 2000) and canopy height (Riom and LeToan, 1981; Dobson *et al.*, 1995b; Harrell *et al.*, 1997); (iv) flooding and the presence/absence of standing water (Hess *et al.*, 1990; Morrissey *et al.*, 1994; Kasischke and Bourgeau-Chavez, 1997), and (iv)

near-surface soil moisture (French *et al.*, 1996). A detailed review of the use of imaging radars for monitoring terrestrial ecosystems can be found in Kasischke *et al.* (1997). Leblon (2001) reviewed the use of imaging radars for monitoring fuel moisture and fire dangers.

Three sources of moisture variation may contribute to the forest radar backscatter: the forest floor, the canopy (including its woody elements) and the environmental conditions (rain events). Forest floor moisture of boreal forests significantly contributed to σ^0 (Dobson *et al.*, 1992; Rignot *et al.*, 1994; Wang *et al.*, 1994; Harrell *et al.*, 1995; Kasischke *et al.*, 1995a; French *et al.*, 1996; Bourgeau-Chavez *et al.*, 1999; Pulliainen *et al.*, 1994, 1996, 1999; Moghaddam *et al.*, 2000). Canopy moisture variables were related to σ^0 acquired over various forest types (Westman and Paris, 1987; Way *et al.*, 1991; Weber and Ustin, 1991; Vidal *et al.*, 1994; Beaudoin *et al.*, 1995; Moghaddam and Saatchi, 1999; Saatchi and Moghaddam 2000; Leblon, 2001). Moghaddam and Saatchi's studies used data acquired over a pine stand with low biomass, for which the seasonal σ^0 variation can also be attributed to forest floor moisture variations. Indeed, for similar stands, Wang *et al.* (1994) showed that σ^0 variation due to soil moisture variation was on the same order of magnitude than the one observed by Moghaddam and Saatchi (1999). Finally, rain events increased σ^0 when they occurred prior to image acquisition (Rignot *et al.*, 1994; Pulliainen *et al.*, 1996, 1999; Bourgeau-Chavez *et al.*, 1999), but decreased σ^0 when they occurred during image acquisition, because of attenuation by rain (Pulliainen *et al.*, 1996) and possible specular scattering by water droplets to the incoming radar energy.

3. Materials and Methods

3.1. STUDY AREA

Our study area is located in the Mackenzie River basin (Northwest Territories, Canada), between 57°39′ and 71°27′ North Latitude and 110°39′ and 135°18′ West Longitude (Figure 1). Forests located in this region experienced a high fire occurrence between 1980 and 1989 and in 1994 (Gallant, 1998). It is predicted that annual area burned in the basin will increase, and by 2050 reach 150% of the level of 1980 (Rothman and Herbert, 1997). These predictions resulted from the combination of (i) the actual ratio between burned areas and the Fire Weather Index (Canadian Forest Service, 1987) (estimated from historical data between 1951 and 1980 for the Yellowknife and Fort Smith areas) with (ii) the predictable changes in temperatures and precipitations (using the Goddard Institute Space Studies general circulation model assuming a doubling of atmospheric CO_2). The prediction assumed climate warming will not affect fire ignition probability.

Our study area falls within the Taiga Plains Ecozone of Canada, and includes the transitional, the boreal (taiga), and the mixed and deciduous forest zones of the land cover map of Canada (Figure 1). Ground measurements were performed on stands located at different sites (Figure 1) selected using the following criteria: (a)

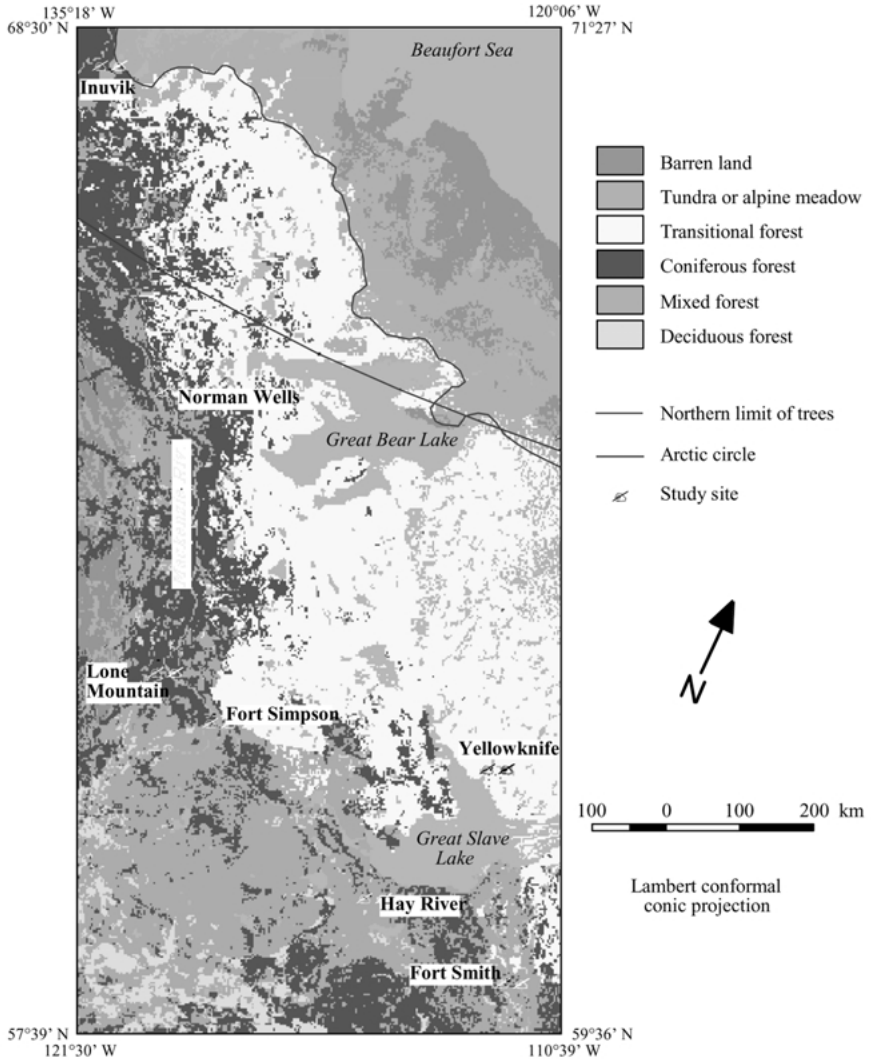

Figure 1. Location of the study sites on a vegetation map derived from a NOAA-AVHRR image (after Gallant, 1998).

proximity of a weather station; (b) accessibility for field sampling; (c) variations in latitude, longitude and elevation. All sites were located in the boreal or mixed forest zones of Figure 1, except the Yellowknife site, which was in the transitional forest zone. The stands also varied in terms of the composition of the coniferous overstory (Table I).

While it would have been desirable to have a distribution of test stands that are proportional to the area covered by each forest type within the study region, funding limitations restricted the degree of sampling that could be reasonably achieved.

Table I. Geographical and biological characteristics of the studied sites (classified from the southern part to the northern part of the study area)

Site[1]	Weather station							Stand							
	Name & number [2]	Lat. N.	Long W.	Elev. (m)	Lat. N.	Long. W.	Elev. (m)	Overstory[3]	Understory[4]	FMC period	DBH[5] (cm)	CBH[6] (m)	H[7] (m)	N[8]	Density (stem/ha)
FS	FS(A)	60°01′	111°57′	205	60°00′36″	112°12′11″	185	JP	A	30/04–13/10	18.4 ±8.3	2.32 ±1.02	12.3 ±2.9	10	410
	2202200				60°00′54″	112°15′04″	185	BS	LT	30.04–13/10	8.2 ±1.3	1.58 ±0.21	6.3 ±1.1	10	5857
					60°03′45″	112°13′06″	180	WS	W, DB	30/04–13/10	14.8 ±9.8	1.78 ±0.64	11.3 ±5.2	10	1882
HR	HR(A)	60°50′	115o47′	166	60o30′28″	116°14′47″	275	JP	W, A	30/04–13/10	18.7 ±4.0	3.31 ±2.37	12.9 ±2.2	10	622
	2202400				60°30′31″	116°14′57″	275	BS	LT	30/04–13/10	18.7 ±9.1	0.79 ±0.70	11.6 ±3.9	10	975
					60°33′32″	116°07′51″	250	WS	Nothing	30/04–13/10	17.3 ±4.4	3.73 ±3.23	12.3 ±2.8	4	2077
SF	SF(A)	61°45′	121°14′	169	61°52′05′	121°28′24″	130	JP	DB (close)	01/05–15/09	19.6 ±2.6	1.46 ±0.67	12.0 ±1.6	5	1328
	2202101				61°53′04″	121°37′52″	130	WS	W, A	01/05–15/09	23.4 ±1.1	1.90 ±0.82	14.3 ±3.2	5	1470
					61°56′33″	$121^{circ}33'53''$	130	BS	LT	01/05–15/09	14.8 ±2.1	1.48 ±0.45	10.5 ±1.1	5	2148
LM	LOMO	61°11′	123°20′	686	62°11′18″	123°20′05″	686	WS	DB, LT,	10.06–01/09	28.8 ±1.4	n/a	10.7 ±2.1	3	n/a
					62°11′18″	123°20′05″	686	IP	W, A	10/06–01/09	21.5 ±0.7	n/a	4.7 ±0.5	2	n/a
YK	YK(A)	62°28′	114°27′	206	60°31′36″	114°10′52″	183	WS	Nothing	01/05–15/09	13.1 ±1.5	1.60 ±0.51	10.9 ±0.8	5	2120
	2204100				62°31′37″	114°10′52″	183	BS	LT	01/05–15/09	10.5 ±1.3	n/a	n/a	5	2120
					62°31′50″	114°09′15″	168	JP	W, A	01/05–15/09	11.0 ±1.5	1.64 ±0.19	6.3 ±0.7	5	1554

Table I. Continued

Site[1]	Weather station							Stand							
	Name & number [2]	Lat. N.	Long W.	Elev. (m)	Lat. N.	Long. W.	Elev. (m)	Overstory[3]	Understory[4]	FMC period	DBH[5] (cm)	CBH[6] (m)	H[7] (m)	N[8]	Density (stem/ha)
NW	NW(A)	65°17′	126°48′	74	65°16′27″	126°45′35″	69	BS	W, LT	05/05–05/09	6.1 ±1.4	0.72 ±0.65	4.7 ±1.4	5	5546
	2202800				65°17′27″	126°52′30″	61	WS	DB, A	05/05–05/09	12.9 ±3.3	2.11 ±0.99	11.4 ±2.4	10	8953
IN	IN(A)	68°18′	133°29′	68	68°18′54″	133°31′01″	69	WS	DB	15/05–20/09	6.0 ±1.6	0.56 ±0.48	8.3 ±1.4	5	1244
	2202570				68°19′43″	133°37′39″	23	BS	W, A, LT	15/05–20/09	2.9 ±0.6	0.00 ±0.00	4.4 ±1.4	5	1004

[1]FS = Fort Smith, YK = Yellowknife, HR = Hay River, SF = Fort Simpson, LM = Lone Mountain, NW = Norman Wells, IN = Inuvik, [2]Weather station located at the airport and operated by Environment Canada (except for Lone Mountain, where the weather station is located on the Lone Mountain tower and is operated by the Northwest Territories Department of Natural Resouces); [3]WS = white spruce, BS = black spruce, JP = jack pine, [4]DB = dwarf birch; LT = Labrador tea; W = willow, A = alder; [5]DBH = Diameter at breast height (mean ± standard deviation); [6]CBH = height of the crown basis (mean ± standard deviation); [7]H = tree height (mean ± standard deviation); [8]N = number of sampled trees.

The stands used in this study are representative of the forests found in the study area and are located on sites well distributed throughout the study area (Figure 1). The stands were selected to not include deciduous tree species, because seasonal variations in leaf biomass could affect the radar backscatter signature independent of variations in fuel moisture.

3.2. MATERIALS AND METHODS

Our study used data acquired during the 1994 fire season. FWI codes and indices were computed from dry-bulb air temperature, relative humidity, wind and precipitation data acquired at the weather stations nearest to the study stands (Table I). The computation was done using the WeatherProTM package of Remsoft Inc., which is based on the method detailed in Canadian Forest Service (1987).

Characteristics of the overstory trees in each stand were measured, including tree density, tree height, diameter at breast height and foliar moisture content (based on samples of canopy foliage). Each site covered an area of 10 ha, and consisted of pure stands of white spruce *(Picea glauca (Moensch) Voss)*, black spruce *(Picea mariana (Mill.) B.S.P.)* or jack pine *(Pinus banksiana Lamb.)* (Table I). In each stand, separate samples of new, 1-year and 2-year needles were collected weekly, beginning from the date of snow melt to the date of the first snowfall. From these samples, foliar moisture content (in % dry weight) was determined by measuring fresh and dry weights. Only FMC's higher than 70% (% dry weight) were further considered, because a lower value corresponds to dying needles that do not remain on the branches. As already observed over coniferous stands located elsewhere in Canada, seasonal variation of new foliage FMC in spring considerably differs from those of old foliage FMC (Van Wagner, 1967; Canadian Forest Service, 1992). In spring, as the foliage weight increases with the spring growth, FMC of new foliage sharply declines and converges to a similar moisture content as the old foliage. During the same period, old foliage FMC decreases to a minimum before the new growth flushes and then increases to a relatively constant value. This variation is known as the spring dip (Van Wagner, 1967; Canadian Forest Service, 1992).

For this reason, two kinds of FMC were considered in the study. The first, referred hereafter as "old foliage FMC or FMC_{old}", is the FMC considered in the CFFDRS method, i.e., the simple mean between FMC of 1-year and 2-year needles. The second is a composite FMC value, which also accounts for new foliage FMC. Indeed, spaceborne measurements are also sensitive to new needles that are located towards the crown outside, while old needles are located within the crown. The new needle FMC is included into the composite FMC value (FMC_{comp}) by considering a weighting factor, as follows (adapted from Nugroho, 1999):

$$FMC_{comp} = (FMC_n \times \%n) + (FMC_{old} \times (100 - \%n)) \quad (1)$$

where FM_{comp} = FMC (% dry weight) of the composite foliage; FMC_n = FMC (% dry weight) of the new foliage; FMC_{old} = FMC (% dry weight) of the old foliage; %n = part of the new foliage within the crown (%).

The part of the new foliage within the total foliage (%n) is assumed to increase from early spring to the end of the spring dip period, as follows:

(1) for the period before the end of spring dip ($t \leq t_e$) (Nugroho, 1999):

$$\%\mathrm{n} = \frac{(t - t_s)}{(t_e - t_s)} \times \text{constant} \tag{2}$$

with t = observed Julian date; t_s = Julian date of the snowmelt; t_e = Julian date of the end of the spring dip; constant = 20% for the spruce and 33% for the jack pine (Van Wagner, 1967).

(2) for the period after the end of spring dip ($t > t_e$) (Van Wagner, 1967):

$$\%\mathrm{n} = \text{constant} \tag{3}$$

with constant = 20% for the spruce and 33% for the jack pine (Van Wagner, 1967).

Radar image intensities were extracted from twenty-two ERS-1 SAR images recorded and calibrated by the Alaska SAR facility (ASF) in Fairbanks, AK (Table II) using the procedures detailed in Fatland and Freeman (1992). The images were acquired under the weather conditions listed in Table II. The images have a nominal ground resolution of 30 m.

Only daytime ERS-1 SAR images (descending orbit) were used because they were acquired close to the time when weather data were recorded to estimate FWI indices (Table II). Each ERS-1 SAR image was processed using the EASI/PACE image analysis package, according to the procedure detailed in Nugroho (1999). The image processing includes: (i) image downloading, (ii) subset image creation based on the image corners' coordinates, (iii) geometric corrections and (iv) radar backscatter (σ^0) computation by the following equation (adapted from Nugroho, 1999):

$$\sigma^0 = 10 \times \log_{10}(a_2 \times DN^2 + a_3) \tag{4}$$

where σ^0 = radar backscatter (in dB); DN = digital number; a_2 = noise scaling factor provided through the trailer file and depending on the receiving station (1.2E − 5 for ASF); a_3 = offset scaling factor provided through the trailer file and depending on the receiving station (0.0E + 0 for ASF).

Radar image intensity is measured in a log scale because of the large dynamic range exhibited in this data type (values can vary by two to three orders of magnitude within a single scene). For reference purposes, if two radar backscatter measurements are 1 dB different, then they vary by a factor of 1.25, if they are 2 dB different, they vary by a factor of 1.6, and if they are 3 dB different, they vary by a factor of 2.0.

Table II. Weather conditions, radar backscatters and corresponding FMC and FWI codes and indices for each image

Site[1]	Sp.[2]	Julian	Days snow	σ^0 (dB)[3]	Time (LT)	P (mm)[4]	ΣP (mm)[5]	T_{max} (°C)[6]	Rh (%)	FFMC	DMC	DC	BUI	FWI	Danger class[8]	Julian	Days snow	FMC_{old}	FMC_{comp}
FS	JP	216	96	−10.88	12:38	0.0	0.40	25.0	48.6	90.2	77.0	464.0	108.8	22.9	Very high	217	97	98.85	116.90
		236	116	−8.80	12:36	15.00	17.22	10.0	94.1	20.6	46.1	507.0	75.1	0.0	Very low	237	116	108.96	125.80
		253	133	−9.57	12:39	10.20	17.00	7.9	94.9	17.5	17.2	508.0	31.7	0.0	Very low	258	138	108.31	124.94
FS	BS	216	96	−10.85	12:38	0.00	0.40	25.0	48.6	90.2	77.0	464.0	108.8	22.9	Very high	217	97	94.7	97.84
		236	116	−9.11	12:36	15.00	17.22	10.0	94.1	20.6	46.1	507.0	75.1	0.0	Very low	237	116	97.23	101.55
		253	133	−10.87	12:39	10.20	17.00	7.9	94.9	17.5	17.2	508.0	31.7	0.0	Very low	251	131	103.72	106.34
FS	WS	216	96	−8.37	12:38	0.00	0.40	25.0	48.6	90.2	77.0	464.0	108.8	22.9	Very high	217	97	110.56	113.82
		236	116	−7.93	12:36	15.00	17.22	10.0	94.1	20.6	46.1	507.0	75.1	0.0	Very low	237	116	105.01	108.73
		253	133	−7.16	12:39	10.20	17.00	7.9	94.9	17.5	17.2	508.0	31.7	0.0	Very low	251	131	120.15	122.86
HR	JP	153	33	−11.17	12:51	0.00	0.0	22.0	21.9	92.7	51.1	287.8	70.8	40.5	Extreme	152	32	82.47	82.47
		190	70	−9.66	12:51	3.40	3.80	22.9	36.0	82.8	78.5	495.8	112.5	24.5	Very high	187	67	87.78	96.57
	WS	115	33	−9.95	12:51	0.00	0.00	22.0	21.9	92.7	51.1	287.8	70.8	40.5	Extreme	152	32	71.90	71.90
		190	70	−9.72	12:51	3.40	3.80	22.9	36.0	82.8	78.5	495.8	112.5	24.5	Very high	187	67	89.20	100.12
	BS	153	33	−8.96	12:51	0.00	0.00	22.0	21.9	92.7	51.1	287.8	70.8	40.5	Extreme	159	39	78.81	78.81
		190	70	−10.21	12:51	3.40	3.80	22.9	36.0	82.8	78.5	495.8	112.5	24.5	Very high	187	67	85.62	96.21
SF	JP	155	34	−9.94	13:20	0.00	0.00	23.6	36.3	92.1	24.9	340.3	42.2	19.6	Very high	158	37	89.51	112.08
		175	54	−9.59	13:18	4.40	8.80	15.5	48.2	60.4	17.4	348.1	30.9	0.8	Very low	173	52	92.31	103.52
		192	71	−8.40	13:21	0.00	52.40	23.6	55.2	72.2	10.2	268.2	18.6	1.3	Very low	194	73	100.25	118.78
	WS	155	34	−10.43	13:20	0.00	0.00	23.6	36.3	92.1	24.9	340.3	42.2	19.6	Very high	158	37	85.86	107.29
		175	54	−9.01	13:18	4.40	8.80	15.5	48.2	60.4	17.4	348.1	30.9	0.8	Very low	173	52	83.50	96.77
		192	71	−9.51	13:21	0.00	52.40	23.6	55.2	72.2	10.2	268.2	18.6	1.3	Very low	194	73	92.51	100.80
		229	108	−10.97	13:22	0.00	0.00	21.5	59.5	85.1	96.9	536.1	133.5	14.7	High	228	107	103.07	111.4
	BS	155	34	−9.99	13:20	0.00	0.00	23.6	36.3	92.1	24.9	340.3	42.2	19.6	Very high	158	37	82.58	96.51
		175	54	−8.44	13:18	4.40	8.80	15.5	48.2	60.4	17.4	348.1	30.9	0.8	Very low	173	52	83.22	98.29
		192	71	−10.03	13:21	0.00	52.40	23.6	55.2	72.2	10.2	268.2	18.6	1.3	Very low	194	73	93.07	98.09
		229	108	−10.79	13:22	0.00	0.00	21.5	59.5	85.1	96.9	536.1	133.5	14.7	High	228	107	100.87	102.77
YK	WS	173	52	−9.85	12:48	0.00	1.20	16.0	56.0	84.5	71.7	453.9	102.8	12.6	High	174	53	94.01	105.51
		190	69	−9.17	12:51	0.10	6.00	19.0	65.0	80.9	43.1	499.1	70.8	11.9	High	189	68	86.14	97.10
	BS	173	52	−9.85	12:48	0.00	1.20	16.0	56.0	84.5	71.7	453.9	102.8	12.6	High	174	53	85.33	98.32
		190	69	−9.17	12:51	0.10	6.00	19.0	65.0	80.9	43.1	499.1	70.8	11.9	High	189	68	97.54	108.22
	JP	173	52	−7.95	12:48	0.00	1.20	16.0	56.0	84.5	71.7	453.9	102.8	12.6	High	174	53	72.89	80.11
		190	69	−9.49	12:51	0.10	6.00	19.0	65.0	80.9	43.1	499.1	70.8	11.9	High	189	68	74.95	89.88
NW	BS	194	69	−10.33	13:50	0.00	0.00	21.0	38.7	91.5	60.7	454.3	91.0	28.4	Very high	191	66	77.89	84.51
		197	72	−10.87	13:44	0.10	0.10	22.0	53.0	87.4	68.8	477.5	101.2	13.1	High	199	74	87.76	93.86
		217	92	−10.83	13:42	0.00	0.00	21.0	63.3	86.6	54.0	520.6	85.7	15.0	High	219	94	105.94	108.56
		234	109	−10.53	13:45	0.40	0.40	9.0	87.2	81.2	67.0	630.3	105.8	20.8	Very high	233	108	104.87	105.93
		251	126	−10.89	13:48	0.00	4.00	10.0	70.6	70.9	50.0	683.7	84.5	4.2	Low	247	122	98.54	98.66

Table II. Continued

Site[1]	Sp.[2]	Julian	Days snow	σ^0 (dB)[3]	Time (LT)	P (mm)[4]	ΣP (mm)[5]	T_{max} (°C)[6]	Rh (%)	FFMC	DMC	DC	BUI	FWI	Danger class[8]	Julian	Days snow	FMC_{old}	FMC_{comp}
NW	WS	194	69	−9.89	13:50	0.00	0.00	21.0	38.7	91.5	60.7	454.3	91.0	28.4	Very high	191	66	88.08	96.17
		197	72	−8.68	13:44	0.10	0.10	22.0	53.0	87.4	68.8	477.5	101.2	13.1	High	199	74	94.84	101.06
		217	92	−8.98	13:42	0.00	0.00	21.0	63.3	86.6	54.0	520.6	85.7	15.0	High	219	94	109.46	112.76
		234	109	−10.49	13:45	0.40	0.40	9.0	87.2	81.2	67.0	630.3	105.8	20.8	Very high	233	108	107.53	110.68
		251	126	−7.78	13:48	0.00	4.00	10.0	70.6	70.9	50.0	683.7	84.5	4.2	Low	247	122	106.54	108.20
IN	BS	213	78	−9.58	14:22	0.00	0.00	25.4	61.0	85.5	42.3	425.0	67.8	9.3	High	213	78	99.50	100.42
		233	98	−10.52	14:19	0.00	0.00	16.0	66.7	86.2	58.5	545.8	92.2	13.8	High	234	99	106.85	108.86
		250	115	−10.52	14:22	0.00	5.00	8.4	40.0	72.3	11.7	495.0	22.1	0.8	Very low	249	114	102.73	106.30
IN	WS	213	78	−10.29	14:22	0.00	0.00	25.4	61.0	85.5	42.3	425.0	67.8	9.3	High	213	78	101.56	105.14
		233	98	−10.33	14:19	0.00	0.00	16.0	66.7	86.2	58.5	545.8	92.2	13.8	High	234	99	99.20	106.45
		250	115	−9.84	14:22	0.00	5.00	8.4	40.0	72.3	11.7	495.0	22.1	0.8	Very low	249	114	100.04	102.49

[1]FS = Fort Smith, YK = Yellowknife, HR = Hay River, SF = Fort Simpson, NW = Norman Wells, IN = Inuvik, [2]WS = white spruce, BS = black spruce, JP = jack pine; [3]ERS-1 SAR radar backscatter (in dB); [4]Rainfall during 24 hours prior to image acquisition; [5]Cumulative rainfalls during 72 hours prior to image acquisition; [6]Dry-bulb air temperature at noon time; [7]Relative humidity at noon time; [8]Ranking based on FWI values according to Canadian Forest Service (1987).

Each stand was then located on the georeferenced images and a 10 by 10 sampling window was extracted for each study stand. This window size is statistically large enough to remove speckle effect from the computed radar backscatters (French, 1996), while at the same time, preserving the average σ^0 values. Radar backscatters were then compared to climate parameters, computed FWI codes and indices and measured FMC using the regression and correlation procedures of the SAS statistical package.

4. Results and Discussions

4.1. SEASONAL VARIATION OF σ^0

Our initial examination of the radar imagery collected around the Lone Mountain sites showed that the radar backscatter from this region might be affected by topographic influences, e.g., shadowing and radar layover (e.g., Franklin *et al.*, 1995). Because of this effect, the data from these sites were not used in this analysis.

Average σ^0 values for each individual stand for all dates ranged between -7.77 dB for the white spruce stand in Fort Smith and -10.61 dB for the black spruce stand in Norman Wells (Table III). The range of seasonal variation in σ^0 was between 0.23 dB for the white spruce at Hay River and 2.70 dB for the white spruce stand at Norman Wells (Table III). At the site level, average σ^0 values for all dates ranged between -9.25 dB in Yellowknife and -10.18 dB in Inuvik (Table III). On average, per site, the range of seasonal variation in σ^0 was between 0.72 dB in Iunvik and 1.95 dB in Fort Simpson. Average σ^0 values for all stands and all dates for the three different forest types were -10.01 dB for black spruce, -9.41 dB for white spruce and -9.55 dB for jack pine. On average, per species, the range of seasonal variation in σ^0 was 1.26 dB for black spruce, 1.21 dB for white spruce and 1.67 dB for jack pine. Overall, the average σ^0 value was -9.67 dB, but the σ^0 values ranged between -7.16 to -11.17 dB for all the different stands over the entire growing season. On average, the range of seasonal variation in σ^0 was 1.34 dB.

The observed ranges of variation were similar to those observed with ERS-1 C-VV SAR images over unburned Alaska spruce forests (0.8 to 2.0 dB in Rignot *et al.*, 1994; Harrell *et al.*, 1995; Kasischke *et al.*, 1995; Bourgeau-Chavez *et al.*, 1999) and with JPL AIRSAR polarimetric images over jack pine stands at the southern BOREAS site (1.46 to 2.8 dB in Moghaddam and Saatchi, 1999; Moghaddam *et al.*, 2000).

4.2. INFLUENCE OF WEATHER CONDITIONS ON SEASONAL VARIATION OF σ^0

For this analysis, we assumed that the rainfall and temperatures observed at weather stations near the site were indicative of the overall climate conditions of the test sites. Figure 2 presents a plot of three weather parameters: (i) daily dry-bulb air temperatures (Figure 2a), (ii) rainfall accumulated during 24 hours prior to image

Table III. Mean, maximum, minimum and range of variation (in dB) of ERS-1 C-VV backscatters observed over the studied sites

Site[1]	Species[2]	Mean	Max	Min	Range	M[3]
FS	BS	−10.28	−9.11	−10.87	1.76	3
	WS	−7.82	−7.16	−8.37	1.21	3
	JP	−9.75	−8.80	−10.88	2.08	3
	Mean	−9.28	−8.36	−10.04	1.68	3
HR	BS	−9.59	−8.96	−10.21	1.25	2
	WS	−9.83	−9.72	−9.95	1.25	2
	JP	−10.41	−9.65	−11.17	1.51	2
	Mean	−9.94	−9.45	−10.44	1.00	2
SF	BS	−9.81	−8.44	−10.79	2.35	4
	WS	−9.98	−9.01	−10.97	1.96	4
	JP	−9.31	−8.40	−9.94	1.54	3
	Mean	−9.70	−8.62	−10.57	1.95	4
YK	BS + WS	−9.51	−9.17	−9.85	0.68	2
	JP	−8.72	−7.95	−9.49	1.54	2
	Mean	−9.25	−8.76	−9.73	0.96	2
NW	BS	−10.69	−10.33	−10.89	0.56	5
	WS	−9.16	−7.78	−10.48	2.70	5
	Mean	−9.93	−9.06	−10.69	1.63	5
IN	BS	−10.20	−9.58	−10.52	0.95	3
	WS	−10.15	−9.84	−10.33	0.49	3
	Mean	−10.18	−9.71	−10.43	0.72	3
Mean	BS	−10.01	−9.27	−10.52	1.26	3
	WS	−9.41	−8.78	−9.99	1.21	3
	JP	−9.55	−8.70	−10.37	1.67	3
	Mean	−9.67	−8.94	−10.29	1.34	3

[1]FS = Fort Smith, YK = Yellowknife, HR = Hay River, SF = Fort Simpson, NW = Norman Wells, IN = Inuvik, Mean = mean amongst all the sties; [2]WS = white spruce, BS = black spruce, JP = jack pine; Mean = mean amongst all the species; [3]Number of cases (images × dates) (one image can have several stands).

acquisition (Figure 2b) and (iii) rainfall accumulated during 72 hours prior to image acquisition (Figure 2c). Each parameter was collected measured at noon local time, 1 to 3 hours prior to the ERS-1 overpasses over the study sites (Table II).

Radar backscatter (σ^0) exhibits a decreasing trend with increasing air temperatures (Figure 2a). Several studies already interpreted seasonal σ^0 variations in

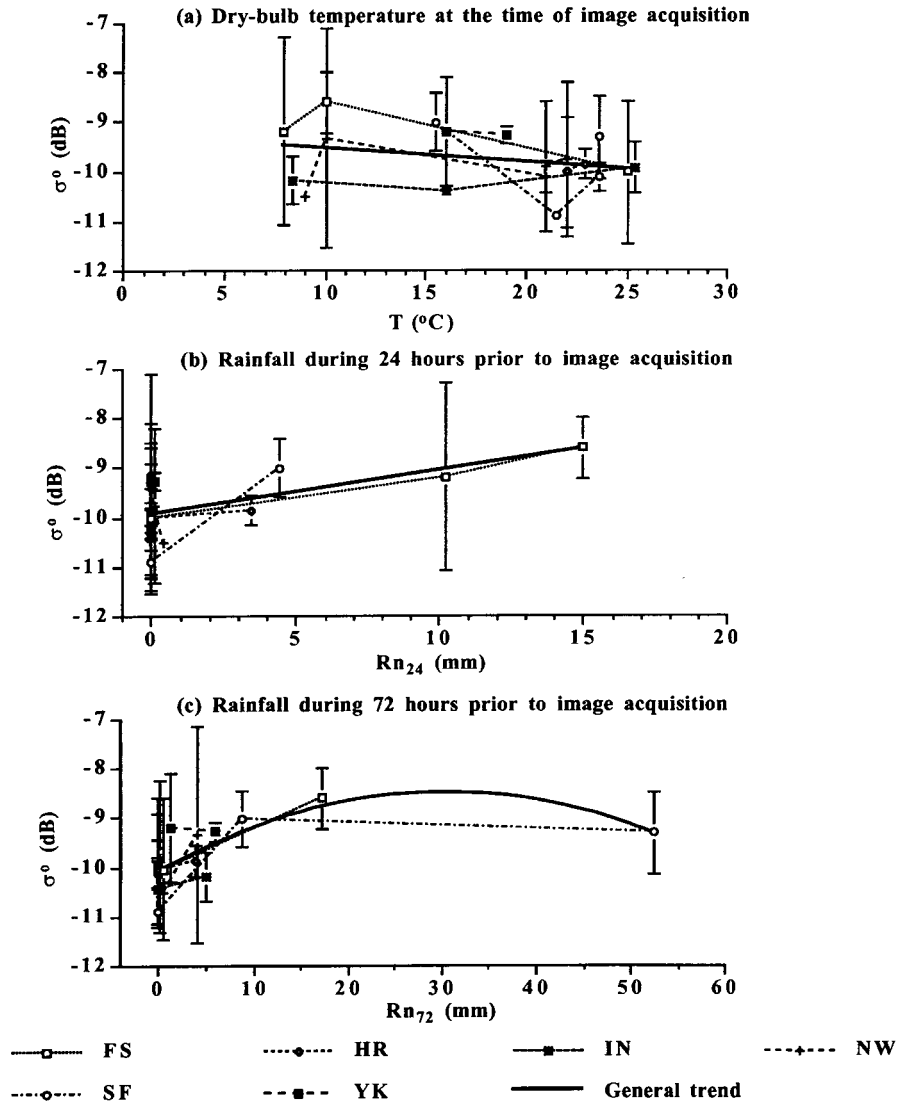

Figure 2. Plots of σ^0 versus daily weather data for (a) dry-bulb air temperature during image acquisition; (b) rainfall during 24 hours prior to image acquisition and (c) cumulative rainfall during 72 hours prior to image acquisition.

terms of air temperature fluctuations (Moghaddam and Saatchi, 1999; Bourgeau-Chavez *et al.*, 1999). Bourgeau-Chavez *et al.* (1999) found a similar decreasing trend between non-freezing air temperatures and ERS-1 SAR backscatters acquired over Alaska burned and unburned black spruce forests. These authors explained this negative trend by the fact that high air temperatures induces plant water stress

that can lower radar backscatter from the canopy. For our study area, 1994 was shown to be exceptionally dry and hot (Gallant, 1998).

Precipitation was described in two ways: (a) Rn_{24} is the rainfall for the last 24 hours prior to image acquisition; and (b) because rainfall can affect soil moisture (and hence σ^0), which dries over a longer-time frame than 24 hours, the 3-day cumulative rainfall prior to image acquisition (Rn_{72}) was also examined (see, e.g., Pulliainen *et al.*, 1996). For each case, there is the suggestion that σ^0 increases with the rainfall (Figures 2b and c). Bourgeau-Chavez *et al.* (1999) observed an increase in ERS-1 SAR radar backscatter until about 20 mm cumulative rainfall, but then the backscatter remained constant until 30 mm cumulative rainfall.

4.3. RELATIONSHIP BETWEEN σ^0 AND FWI CODES AND INDICES

Table IV summarizes the correlation coefficients between radar backscatter and the various FWI codes and indices. The data in Table IV showed that within the individual regions, there was no systematic relationship between the FWI codes observed radar backscatter. In some regions (Fort Simpson and Alaska, for example), significant relationships do occur, but in most regions, none exist. Fort Simpson was already shown to be the site, where the cumulative precipitation before image acquisition (Rn_{72}) was the highest (Table II). This site also experienced the highest amount of rainfall accumulated throughout the fire season. At this site, the correlation was the highest for BUI ($r = -0.720$) and the lowest for DC ($r = -0.647$) (Table IV).

When one examines correlation coefficients when specific forest types are considered across all regions, some significant patterns emerge. First, within black spruce stands, there does appear to be statistically significant correlations between radar backscatter and the duff moisture code (DMC), drought code (DC), and build up index (BUI), with backscatter decreasing as each of these codes increases (Figure 3). Second, there appears to be a significant relationship between radar backscatter measured in white spruce stands and the fine-fuel moisture code (FFMC), again with radar backscatter decreasing as the FFMC increases (Figure 4). Finally, for the jack pine stands, a significant correlation between σ^0 and the fire weather index, with σ^0 decreasing as FWI increases (Figure 5). The significant relationships between σ^0 and the DMC and DC in the black spruce stands is logical from the standpoint of the physical principles of radar scattering. In the Northwest Territories and Alaska, black spruce stands have open canopies, with much of the ground layer exposed to the incoming microwave radiation. Therefore, variations in the moisture conditions of the ground layer would be expected to alter the amount of energy scattered from these surfaces. The variations in ground surface moisture that the radar is sensitive to also result in changes in the DMC and DC.

It seems, therefore, that σ^0 is sensitive either to fast-drying fuels, in the case of white spruce and jack pine stands, or to slow-drying fuels, in the case of black spruce stands. However, the lack of relationships with one or another type of FWI

Table IV. Pearson's correlation coefficient (R)[1] and the corresponding p-values (p) for the correlation between and FWI indices and codes

Site[2]	Species	FFMC		DMC		DC		BUI		FWI		N
		R	*p*	*R*	*p*	*R*	*p*	*R*	*p*	*R*	*p*	
FS	ALL	−0.403	0.2819	−0.270	0.4823	0.407	0.2774	−0.236	0.5412	−0.410	0.2725	9
HR	ALL	−0.123	0.8162	0.123	0.8162	0.123	0.8162	0.123	0.8162	−0.123	0.8162	6
SF	ALL	**−0.695**	0.0176	**−0.714**	0.0136	**−0.647**	0.0316	**−0.720**	0.0125	**−0.697**	0.0172	11
YK	ALL	0.049	0.9259	0.049	0.9259	−0.049	0.9259	0.049	0.9259	0.049	0.9259	6
NW	ALL	−0.191	0.5981	−0.239	0.5061	0.085	0.8151	−0.253	0.4802	−0.303	0.3955	10
IN	ALL	−0.019	0.9708	−0.188	0.7218	−0.565	0.2427	−0.190	0.7189	−0.188	0.7218	6
AK	BS	−0.282	0.3082	**−0.777**	0.0007	−0.448	0.0938	**−0.754**	0.0012	**−0.639**	0.0103	15
NWT	BS	−0.144	0.5565	−0.335	0.1604	**−0.560**	0.0127	−0.352	0.1393	−0.010	0.9684	19
NWK + AK	BS	−0.143	0.4196	***−0.547***	0.0008	***−0.636***	0.0001	***−0.564***	0.0005	−0.234	0.1822	
NWT	WS	**−0.679**	0.0014	−0.264	0.2747	−0.211	0.3866	−231	0.3420	−0.445	0.0563	19
NWT	JP	−0.325	0.3593	−0.185	0.6095	−0.150	0.6799	−0.151	0.6776	***−0.694***	0.0261	10
NWT	ALL	−0.395	0.0055	−0.257	0.0775	−0.074	0.6192	−0.243	0.0962	−0.344	0.0166	48
NWT + AK	ALL	−0.356	0.0042	−0.342	0.0061	−0.173	0.1753	−0.328	0.0086	−0.379	0.0022	63

[1]Coefficients in bold are significant at $\alpha = 0.05$; cases corresponding to coefficients in italic are plotted in Figures 3, 4, and 5; [2]AK = Alaska data (Bourgeau-Chavez *et al.*, 1999) and NWT = Northwest Territories data (this study).

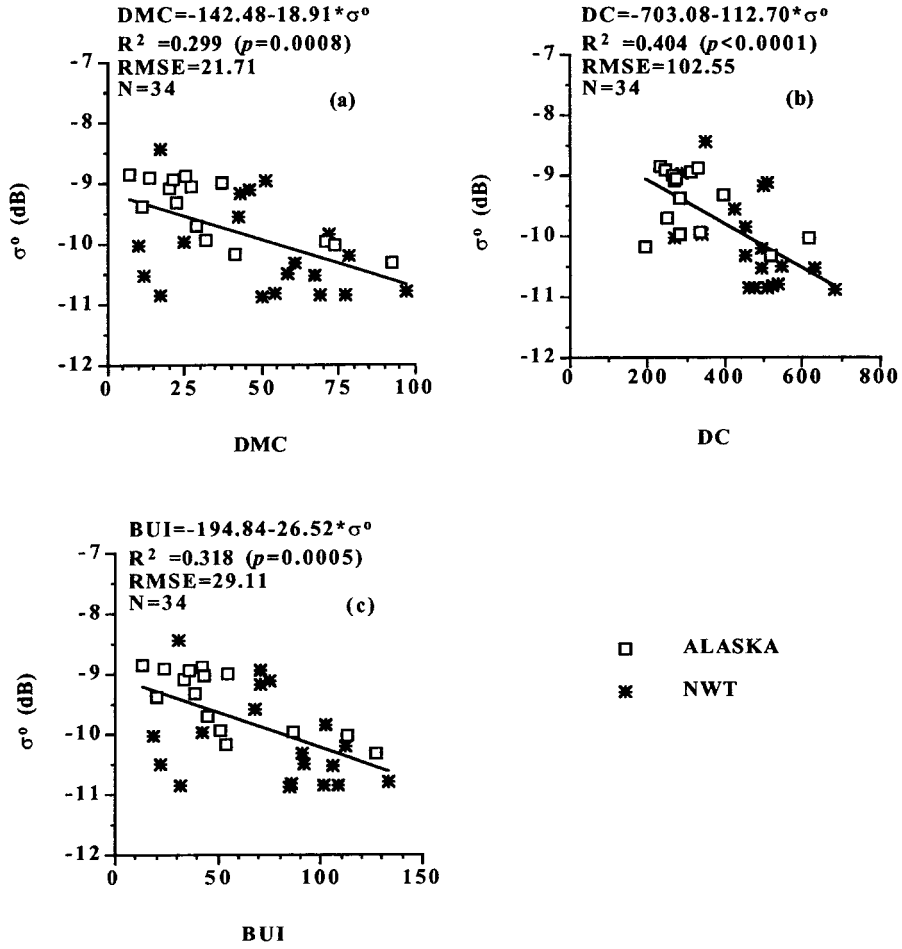

Figure 3. Relationship between σ^0 and slow-drying fuel moisture codes and indices for the black spruce stands located both in Alaska and in Northwest Territories. Data acquired over Alaska stands are from Bourgeau-Chavez et al. (1999). The regression relationships were derived from the combined dataset.

indices may preclude the use of ERS-1 radar backscatters to predict fire danger. Indeed, according to Stocks *et al.* (1989), single FWI codes alone cannot be used to describe fire danger and should be considered all together to predict fire danger, because each code represents a different fire feature. FFMC drives surface litter fire spread, whereas DMC drives the contribution of duff to frontal fire intensity and DC, the ground fire persistence.

Since FWI is the index used for ratings the fire danger "very low" to "extreme" (as described in Canadian Forest Service, 1987), we also computed average σ^0 values for each fire class. These values tend to decrease as the fire danger increases (Figure 6).

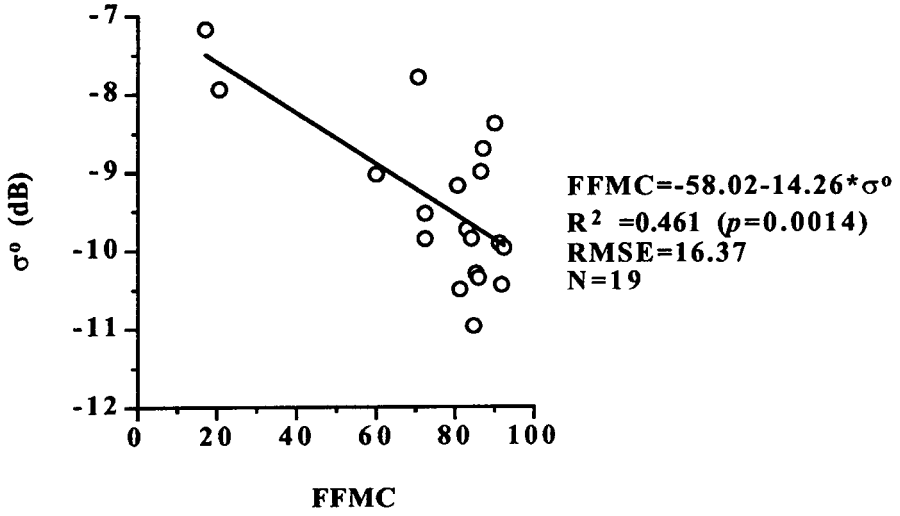

Figure 4. Relationship between σ^0 and FFMC for white spruce stands.

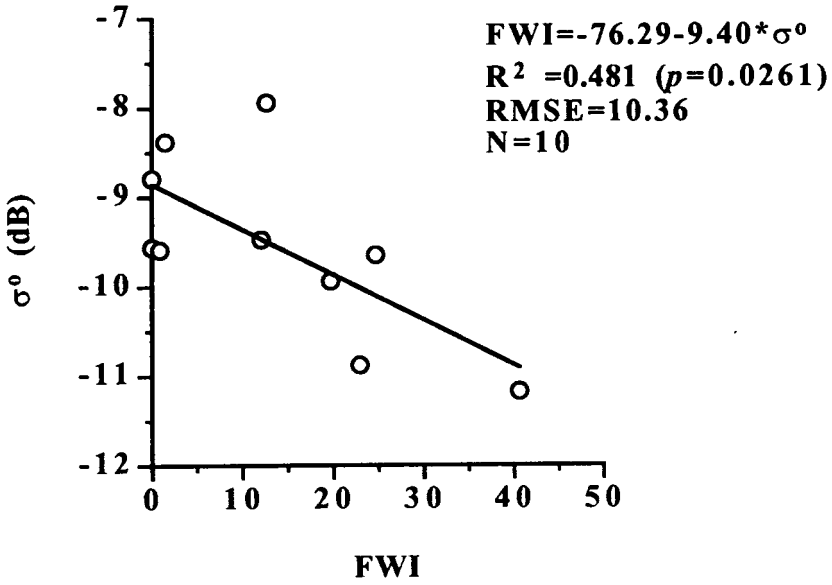

Figure 5. Relationship between σ^0 and FWI for jack pine stands.

4.4. RELATIONSHIP BETWEEN σ^0 AND FMC

As reviewed in the introduction, σ^0 of forested areas depend not only on canopy moisture, but also on (i) vegetation type, species and structure; (ii) vegetation biomass; (iii) surface roughness, i.e., topography and canopy height and (iv) surface moisture. However, for a given stand, the three first factors can be assumed to be relatively time constant, at least over a fire season. The effects of these factors can be

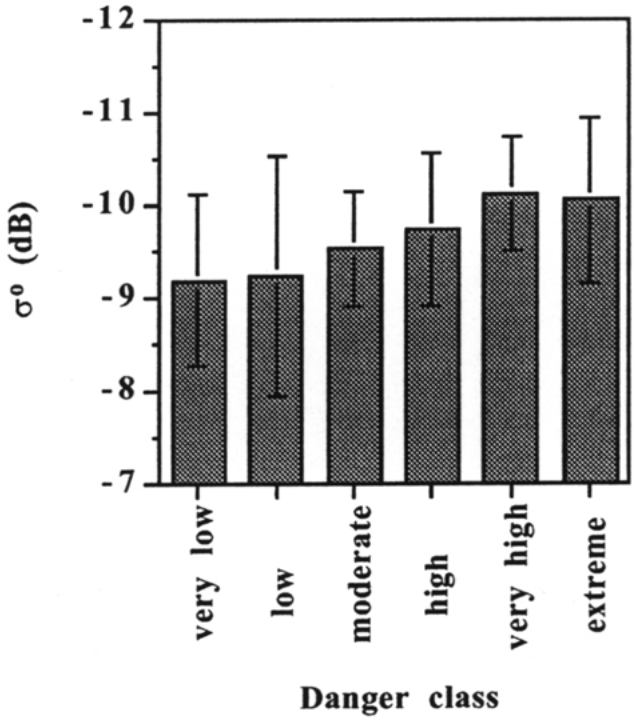

Figure 6. Variation of mean σ^0 as a function of fire danger class (the vertical bar shows one standard deviation).

largely accounted for in the relationship between rates of change in $\sigma^0(\Delta\sigma^0/\Delta t)$ and rates of change in FMC (ΔFMC/Δt). At the Fort Simpson site, $\Delta\sigma^0/\Delta t$ was significantly correlated to ΔFMC/Δt ($r = -0.917$). At this site, a significant relationship was already observed with FWI codes and indices. It was related to the excessive rainfall amount accumulated at this site during the fire season.

Because vegetation type and structure is largely species-dependent, we pooled the data from all sites together per species. There was a significant linear positive relationship with $\Delta\text{FMC}_{\text{old}}/\Delta t$ for the jack pine stands, if the stand in Yellowknife is not considered (Figure 7c). At this site, the mean tree height, i.e., 6 m is about half of the mean tree height at the other sites, i.e., 12 m (Table I). For $\Delta\text{FMC}_{\text{comp}}/\Delta t$, there was a significant quadratic relationship for the white spruce stands, if Norman Wells data are excluded (Figure 8b). At this site, the stand density was excessively high (8953 stems/ha), compared to the other sites (less than 3000 stems/ha) (Table I).

For both FMC's, there was no significant relationship for the black spruce stands (Figures 7a and 8a). This could be related to the rather narrow tree shape of that species, which increases the importance of the ground effect over the measured radar backscatter. For the white spruce stands, the relationship is significant with

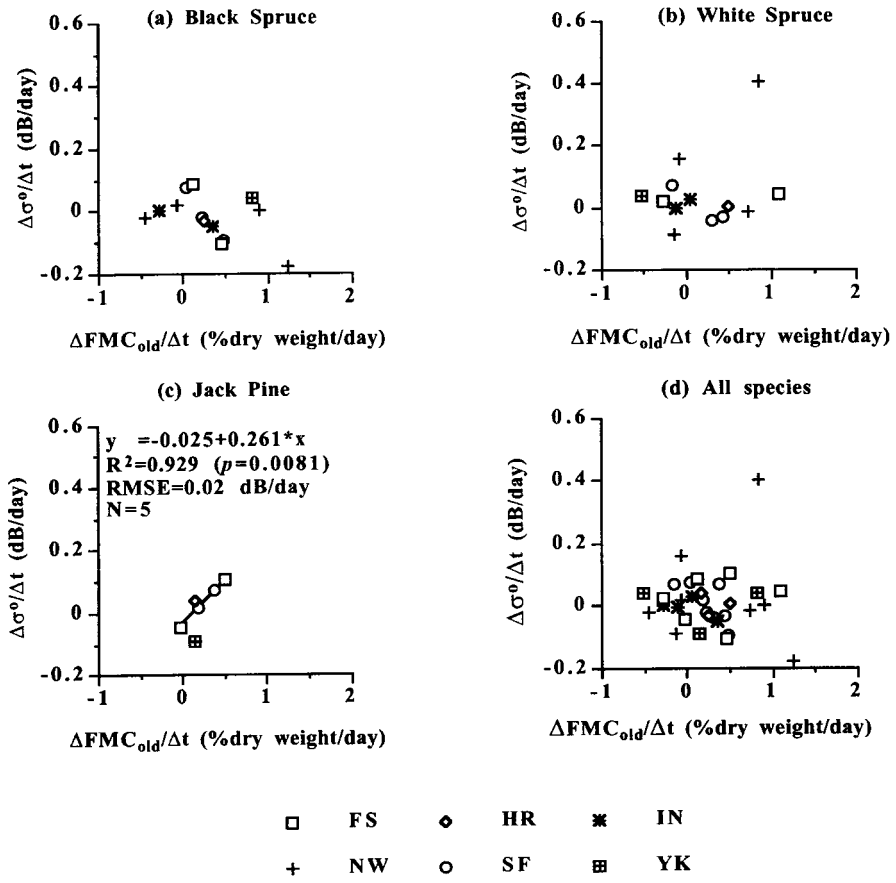

Figure 7. Relationship between rates of change in $\sigma^0(\Delta\sigma^0/\Delta t)$ and rates of change in old FMC ($\Delta\mathrm{FMC}_{\mathrm{old}}/\Delta t$) in the case of the Northwest Territories stands.

$\Delta\mathrm{FMC}_{\mathrm{comp}}/\Delta t$ (Figure 8b), but not with $\Delta\mathrm{FMC}_{\mathrm{old}}/\Delta t$ (Figure 7b). This difference between $\Delta\mathrm{FMC}_{\mathrm{comp}}/\Delta t$ and $\Delta\mathrm{FMC}_{\mathrm{old}}/\Delta t$ can be related to the higher range of variation of $\Delta\mathrm{FMC}_{\mathrm{comp}}/\Delta t$, because of the drastic change in new foliage FMC due to foliage growth (Van Wagner, 1967). For jack pine stands, the significant linear relationship obtained with $\Delta\mathrm{FMC}_{\mathrm{old}}/\Delta t$ on jack pine stands is derived from a small sample (Figure 7c), but jack pine stands have a low density (956.6 stems/ha on average) compared to spruce stands (more than 3000 stems/ha on average) (Table I). The high data scattering with $\Delta\mathrm{FMC}_{\mathrm{comp}}/\Delta t$ in Figure 8c could be related to the influence of highly variable new foliage FMC's in spring due to foliage growth (Van Wagner, 1967).

While both significant relationships were obtained on a small sample size, they are in agreement with previous studies. Relationship between moisture content (in % dry weight) and C-band backscatters were already found using an empirical model over pigmy coniferous forests (Westman and Paris, 1987). Beaudoin *et al.*

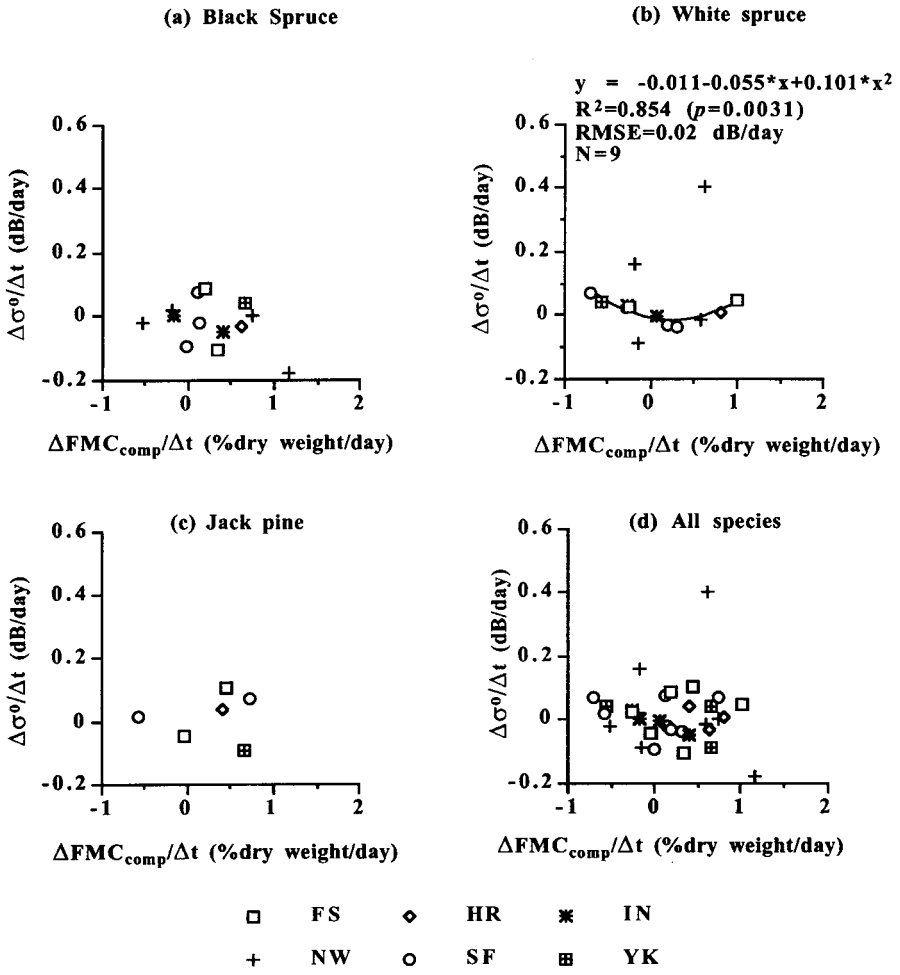

Figure 8. Relationship between rates of change in $\sigma^0(\Delta\sigma^0/\Delta t)$ and rates of change in composite FMC ($\Delta\mathrm{FMC}_{\mathrm{old}}/\Delta t$) in the case of the Northwest Territories stands.

(1995) explained seasonal variations of C-band radar backscatters by change in drought levels over Central France forests, whereas diurnal and day-to-day variations in radar backscatter measured over walnut trees followed changes in water content (Way *et al.*, 1991; Weber and Ustin, 1991). Semi-empirical models were developed to relate radar backscatters to FMC of cork oak stands in French Mediterranean forests and (Vidal *et al.*, 1994), to the moisture content of the young jack pine stand located at the BOREAS Southern study area (Moghaddam and Saatchi, 1999) and to the canopy water content of various BOREAS stands (Saatchi and Moghaddam, 2000).

5. Concluding Remarks

We analyzed the potential use of ERS-1 SAR backscatters (σ^0) for retrieving FWI codes and indices and foliar moisture content (FMC in % dry weight) of coniferous stands located in the Northwest Territories, Canada. Seasonal σ^0 trends were shown to depend somewhat on weather variables like dry-bulb air temperature and the amount of rainfall prior to image acquisition. Relationships were found between σ^0 and FWI codes and indices, in the case of the black spruce stands, between the rate in changes in σ^0 and in FMC_{old}, in the case of jack pine stands and between the rate in changes in σ^0 and in FMC_{comp}, in the case of white spruce stands.

These relationships are only indicative of the potential of ERS-1 images to monitor fuel moisture regimes. First, they were estimated for the year 1994 which was shown to be exceptionally hot and dry in the study area (Gallant, 1998). Second, the revisiting period of ERS-1 does not allow a daily monitoring of fuel moistures. However, although ERS-1 SAR images give different kind of information than optical or thermal infrared images, they may be used as a complementary source of remotely sensed data when optical and thermal infrared images like those acquired daily by NOAA-AVHRR are not available because of cloudy conditions. There is then the need to develop methods which combine radar images to optical or thermal infrared images.

On the other hand, one may expect to have an improved usefulness of radar images in fire danger monitoring, thanks to the recent availability of sensors having a shorter revisiting period. For example, the 1995 launched Canadian radar satellite, RADARSAT-1, has a revisiting period which allowed daily image acquisition over the Northwest Territories, Canada (Giugni, 2000), but with a different spatial resolution and incidence angle configuration. The use of RADARSAT-1 images in fire danger monitoring will be investigated in a next study. The potential of SAR images in fire danger monitoring will also be improved in the near future with the availability of a new generation of radar sensors, like RADARSAT-2 which will provide data having a finer spatial resolution (up to 3 m) and in a polarimetric mode (CCRS, 1998). Multipolarization and multifrequency SAR images were already shown to be suitable to estimate canopy water content of grasslands (Saatchi *et al.*, 1995) and of boreal forests (Moghaddam and Saatchi, 1999; Saatchi and Moghaddam, 2000).

Acknowledgments

The authors thank Frank Ahern as well as two anonymous reviewers for their helpful comments. This study was funded by research grants from the Canadian Interagency Forest Fire Committee and from the Natural Science and Engineering Research Council, awarded to B. Leblon. ERS-1 SAR data processing and interpretation were greatly helped by Nancy French and Laura Bourgeau-Chavez. ERS-1 SAR acquisition at the Alaska SAR facility was supported by a ESA

grant # AO2.USA135 awarded to E. Kasischke. Weather data were obtained from Normand Bussières, Hardy Granberg, Marty Alexander, and Rick Lanoville.

References

Beaudoin, A., Vidal, A., Desbois, N., and Devaux-Ros, C.: 1995, Monitoring the water status of Mediterranean forest using ERS-1 to support fire risk prevention, in *Proceedings of IGARSS 1995 (Quantitative Remote Sensing for Science and Applications)*, Firenze, Italy, pp. 963–965.

Bourgeau-Chavez, L., Kasischke, E. S., and Rutherford, M. D.: 1999, Evaluation of ERS SAR data for prediction of fire danger in a boreal region, *Int. J. Wildland Fire* **9**(3), 183–194.

Canadian Centre for Remote Sensing:1998, RADARSAT-2: high resolution, multi-polarization, *Remote Sensing in Canada* **26**(1), 1.

Canadian Forest Service: 1987, Canadian Forest Fire Danger Rating System – Users's Guide, Fire Danger Group of the Canadian Forest Service, Ottawa, Ontario, Three-ring binder (unnumbered publication).

Canadian Forest Service: 1992, Development and Structure of the Canadian Forest Fire Behaviour Prediction System, Canadian Forest Service, Information Report ST-X-3, Ottawa, ONT., 63 pp.

Dobson, M. C., Pierce, L., Sarabandi, K., Ulaby, F. T., and Sharik, T.: 1992, Preliminary analysis of ERS-1 SAR for forest ecosystem studies, *IEEE Trans. Geosci. Remote Sens.* **30**(2), 203–211.

Dobson, M. C., Ulaby, F. T., and Pierce, L. E.: 1995a, Land-cover classification and estimation of terrain attributes using synthetic aperture radar, *Remote Sens. Environ.* **51**, 199–214.

Dobson, M. C., Ulaby, F. T., Pierce, L. E., Sharik, T. L., Bergen, K. M., Kellndorfer, J., Kendra, J. R., Li, E., Lin, Y. C., Nashashibi, A., Sarabandi, K. L., and Siqueira, P.: 1995b, Estimation of forest biomass characteristics in northern Michigan with SIR-C/XSAR data, *IEEE Trans. Geosci. Remote Sens.* **33**, 877–894.

Fatland, R. and Freeman, A.: 1992, Calibration and change detection of ASF/ERS-1 SAR image data, in *Proceedings of IGARSS 1992*, Houston, TX, pp. 1164–1166.

Franklin, S. E., Lavigne, M. B., Hunt, E. R., Jr., Wilson, B. A., Peddle, D. R., McDermid, G. J., and Giles, P. T.: 1995, Topographic dependence of synthetic aperture radar imagery, *Computers and Geosciences* **21**, 521–532.

French, N. H. F., Kasischke, E. S., Bourgeau-Chavez, L. L., Harrell, P., and Christensen, N. L., Jr.: 1996, Monitoring variations in soil moisture on fire disturbed sites in Alaska using ERS-1 SAR imagery, *Int. J. Remote Sens.* **17**, 3037–3053.

French, N.: 1996, E-mail of February 7, 1996 to B. Leblon

Gallant, L.: 1998, Suivi, par imagerie NOAA-AVHRR, de l'état hydrique de peuplements de conifères du bassin du fleuve Mackenzie (Territoires du Nord-Ouest) dans une perspective de prévision du danger d'incendie de forêt, M.Sc. thesis, University of Sherbrooke, Sherbrooke, Canada. 104 pp.

Giugni, L.: 2000, E-mail to B. Leblon on May 15, 2000.

Harrell, P. A., Bourgeau-Chavez, L. L., Kasischke, E. S., French, N. H. F., and Christensen, N. L., Jr.: 1995, Sensitivity of ERS-1 and JERS-1 radar data to biomass and stand structure in Alaskan boreal forest, *Remote Sens. Environ.* **54**, 247–260.

Harrell, P. A, Kasischke, E. S., Bourgeau-Chavez, L. L., Haney, E., and Christensen, N. L., Jr.: 1997, Evaluation of approaches to estimating of aboveground biomass in southern pine forests using SIR-C imagery, *Remote Sensing Environ.* **59**, 223–233.

Hess, L. L., Melack, J. M., and Simonett, D. S.: 1990, Radar detection of flooding beneath the forest canopy: A review, *Int. J. Rem. Sens.* **11**(7), 1313–1325.

Kasischke, E. S. and Bourgeau-Chavez, L. L.: 1997, Monitoring south Florida wetlands using ERS-1 SAR imagery, *Photogram. Eng. Remote Sens.* **33**, 281–291.

Kasischke, E. S., Morrissey, L., Way, J. B., French, N. H. F., Bourgeau-Chavez, L. L., Rignot, E., Stearn, J. A., and Livingstone, G. P.: 1995a, Monitoring seasonal variations in boreal ecosystems using multi-temporal spaceborne SAR data, *Can. J. Remote Sens.* **21**(2), 96–109.

Kasischke, E. S., Christensen, N. L., Jr., and Bourgeau-Chavez, L. L.: 1995b, Correlating radar backscatter with components of biomass in loblolly pine forests, *IEEE Trans. Geosci. Remote Sens.* **33**, 643–659.

Kasischke, E. S., Melack, J. M., and Dobson, M. C.: 1997, The use of imaging radars for ecological applications – A review, *Remote Sens. Environ.* **59**, 141–156.

Leblon, B.: 2001, Forest fire hazard monitoring using remote sensing: A review, *Remote Sens. Rev.* **20**(1), 1–57.

Leckie, D. G.: 1990, Synergism of synthetic aperture radar and visible/infrared data for forest type discrimination, *Photogram. Eng. Remote Sens.* **56**(9), 1237–1246.

Moghaddam, M. and Saatchi, S.: 1999, Monitoring tree moisture using an estimation algorithm applied to SAR data from BOREAS, *IEEE Trans. Geosci. Remote Sens.* **37**(2), 901–916.

Moghaddam, M., Saatchi, S., and Cuenca, R. H.: 2000, Estimating subcanopy soil moisture with radar, *J. Geophys. Res.* **105**(D11), 14,899–14,911.

Morrissey, L. A., Livingston, G. P., and Durden, S. L.: 1994, Use of SAR in regional methane exchange studies, *Int. J. Remote Sens.* **15**, 1337–1342.

Nugroho, M.: 1999, Foliar moisture content estimation using ERS-1 SAR images, M.F. thesis. University of New Brunswick, Faculty of Forestry, Fredericton, N.B., Canada. 73 pp.

Pulliainen, J. T., Heiska, K., Hyyppä, J., and Hallikainen, M. T.: 1994, Backscattering properties of boreal forests at the C- and X-bands, *IEEE Trans. Geosci. Remote Sens.* **32**(5), 1041–1050.

Pulliainen, J. T., Mikkelä, P. J., Hallikainen, M. T., and Ikonen, J. P.: 1996, Seasonal dynamics of C-band backscatter with applications to biomasss and soil moisture estimation, *IEEE Trans. Geosci. Remote Sens.* **34**(3), 758–770.

Pulliainen, J. T., Kurvonen, L., and Hallikainen, M. T.: 1999, Multitemporal behavior of L- and C-band SAR observations of boreal forests, *IEEE Trans. Geosci. Remote Sens.* **37**(2), 927–937.

Rignot, E., Way, J. B., McDonald, K., Viereck, L., Williams, C., Adams, P., Payne, C., Wood, W., and Shi, J.: 1994, Monitoring of environmental conditions in taiga forests using ERS-1 SAR, *Remote Sens. Environ.* **49**, 145–154.

Riom, J. and Le Toan, T.: 1981, Relationship between tree height and radar image tone in L-band in the case of maritime pine (*Pinus pinaster* L.) forests, in *Proceedings of the 1st International Colloquoium on Spectral Signatures of Objects in Remote Sensing*, Avignon, France, pp. 455–466.

Rothman, D. S. and Herbert, D.: 1997, The socio-economic implications of climate change in the forest sector of the Mackenzie basin, in S. J. Cohen (ed.), *Final Report of the Mackenzie Basin Impact Study (MBIS)*, Vancouver, B.C., Canada, pp. 225–241.

Saatchi, S. S. and Moghaddam, M.: 2000, Estimation of crown and stem water content and biomass of boreal forest using polarimetric SAR imagery, *IEEE Trans. Geosci. Remote Sens.* **38**(2), 697–709.

Saatchi, S. S., van Zyl, J., and Asrar, G.: 1995, Estimation of canopy water content in Konza Prairie grasslands using synthetic aperture radar measurements during FIFE, *J. Geophys. Res.* **100**(D12), 25481–25496.

Stocks, B. J., Lawson, B. D., Alexander, M. E, Van Wagner, C. E., McAlpine, R. S., Lynham, T. J., and Dubé, D. E.: 1989, The Canadian Forest Fire Danger Rating System: An overview, *For. Chron.* **65**(6), 450–457.

Van Wagner, C. E.: 1967, Seasonal variation in moisture content of eastern Canadian tree foliage and the possible effect on crown fires, Report 1204-11-67-3M, Canadian Forest Service, Petawawa (Ont.).

Vidal, A., Devaux-Ros, C., Beaudoin, A., and Maillet, A.: 1994, Suivi du risque d'incendie de forêt par utilisation IR thermique de Landsat-TM et SAR d'ERS-1, *Études de Géographie Physique* **XXIII**, 45–51.

Wang, Y., Kasischke, E. S., Davis, F. W., Melack, J. M., and Christensen, N. L., Jr.: 1994, The effects of changes in loblolly pine biomass and soil moisture variations on ERS-1 SAR backscatter – A comparison of observations with theory, *Remote Sens. Environ.* **49**, 25–31.

Wang, Y., Kasischke, E. S., Bourgeau-Chavez, L. L., O'Neill K. P., and French, N. H. F.: 2000. Assessing the influence of vegetation cover on soil-moisture signatures in fire-disturbed boreal forests in interior Alaska: Modeled results, *Int. J. Remote Sens.* **21**, 689–708.

Way, J. B., Paris, J., Dobson, M. C., McDonald, K., Ulaby, F. T., Weber, J. A., Ustin, S. L., Vanderbilt, V. C., and Kasischke, E. S.: 1991, Diurnal change in trees as observed by optical and microwave sensors: The EOS synergism study, *IEEE Trans. Geosci. Remote Sens.* **29**(6), 807–821.

Weber, J. A. and Ustin, S. L.: 1991, Diurnal water relations of walnut trees: Implications for remote sensing, *IEEE Trans. Geosci. Remote Sens.* **29**(6), 864–874.

Westman, W. E. and Paris, J. F.: 1987, Detecting forest structure and biomass with C-band multipolarization radar: Physical model and field tests, *Remote Sens. Environ.* **22**, 249–269.